An Advanced Meshless Technique for Large Deformation Analysis of Metal Forming

Y. T. Gu, C. Yan and Prasad K.D.V. Yarlagadda

School of Engineering System, Queensland University of Technology, Brisbane, QLD, Australia

ABSTRACT

The large deformation analysis is one of major challenges in numerical modelling and simulation of metal forming. Although the finite element method (FEM) is a well-established method for modeling nonlinear problems, it often encounters difficulties for large deformation analyses due to the mesh distortion issues. Because no mesh is used, the meshless methods show very good potential for the large deformation analysis. In this paper, a local meshless formulation is developed for the large deformation analysis. The Radial Basis Function (RBF) is employed to construct the meshless shape functions, and the spline function with high continuity is used as the weight function in the construction of the local weak form. The discrete equations for large deformation of solids are obtained using the local weak-forms, RBF shape functions, and the total Lagrangian (TL) approach, which refers all variables to the initial (undeformed) configuration. This formulation requires no explicit mesh in computation and therefore fully avoids mesh distortion difficulties in the large deformation analysis of metal forming. Several example problems are presented to demonstrate the effectiveness of the developed meshless technique. It has been found that the developed meshless technique provides a superior performance to the conventional FEM in dealing with large deformation problems in metal forming.

KEY WORDS: Metal forming, Large deformation, Meshless method, FEM

INTRODUCTION

The finite element formulations of metal forming processes can be classified into three categories (Chen et al., 1998): the Lagrangian formulation, the Eulerian formulation, and the Arbitrary Lagrangian Eulerian (ALE) formulation. In the metal forming analysis, it is the key to deal with the large deformation. Although the finite element method (FEM) is a well-established mesh-based method for modeling large deformation problems, it often encounters difficulties due to the mesh distortion issues. Because the meshless methods do not use mesh (Liu and Gu, 2005), they show very good potential for the large deformation analysis.

Although the concept of meshless was proposed in 1970's, it has been widely applied to mechanical engineering from 1990's. Meshless methods have drawn increasing attention from researchers, and some meshless methods have achieved remarkable progress in real applications. These meshless methods do not require a mesh to discretize the problem domain and boundaries, because their approximate solutions are constructed entirely based on a set of scattered field nodes.

Therefore, they can fully resolve the issue related to the mesh distortion in FEM. A group of meshless methods have been developed including the smooth particle hydrodynamics (SPH) (Gingold and Monaghan, 1977), the element-free Galerkin (EFG) method (Belytschko et al., 1994), the reproducing kernel particle method (RKPM) (Liu et al., 1995), and the point interpolation method (PIM) (Liu and Gu, 2001a, 2005).

In the family of meshless methods, the meshless method based on the local weak-form (Atluri and Shen, 2002) is a well-developed technique including the meshless local Petrov-Galerkin (MLPG) method (Alturi and Shen, 2002; Gu and Liu, 2001a,b;), and the local radial point interpolation method (LRPIM) (Gu and Liu, 2001c; Liu and Gu, 2001b, 2002, 2005). This type of meshless method has many attractive advantages including the straightforward approach algorithm, the good efficiency due to no global numerical integration, and the distinguished computational accuracy. Therefore, recently, this type of meshless techniques has been investigated from the theoretical aspect to application aspect. Some studies have been conducted to explore the possible applications of the local meshless techniques in engineering, for example, they have

been successfully used for the applications of two-dimensional elasto-statics and dynamics, fluid mechanics, and MEMS devices.

In this paper, a local meshless formulation is developed for the large deformation analysis of the metal forming, which is a big challenge for researchers in mechanical engineering. Because no mesh is used in the meshless methods, they show very good potential for the large deformation analysis. The meshless methods based on the global weak-forms have been successfully used in this field. Chen et al. (1996, 1998) and Jun (1996) concluded that the meshless methods of EFG and RKPM are very effective for the large deformation analyses with geometrical nonlinearity, because they avoid mesh distortion issues which often caused in the FEM analysis, especially for some geometrically nonlinear problems with very large deformation, for which FEM will fail to give reasonable solutions due to the large mesh distortions.

However, the study for the large deformation analyses by the meshless methods based on the local weak-forms is few. In this paper, a local meshless formulation based on the radial basis function (RBF) interpolation and the local weak form (Liu and Gu, 2005) is developed for the large deformation problems in the metal forming. The discrete equations for solids are obtained using the local weak-forms, and based on the Total Lagrangian (TL) approach. Several numerical examples of the large deformation analysis are presented to illustrate the performance of the present local meshless method. It is demonstrated that the present meshless technique is very effective for the large deformation analyses, because it fully avoids mesh distortion issues.

MESHLESS APPROACH FOR LARGE DEFORMATION

RBF shape functions

To approximate a function $u(\mathbf{x})$ based on a local interpolation domain Ω_s, the approximation $u^h(\mathbf{x})$ for $u(\mathbf{x})$ is defined in the domain Ω by

$$u^h(\mathbf{x}) = \sum_{i=1}^{n} R_i(r)a_i + \sum_{j=1}^{m} p_j(\mathbf{x})b_j \tag{1}$$

with the constraint condition

$$\sum_{i=1}^{n} p_{ij}(\mathbf{x})a_i = 0, \qquad j=1\sim m \tag{2}$$

where $R_i(r)$ is the radial basis function (RBF), n is the number of nodes in the neighborhood (the local interpolation domain) of $\mathbf{x}$, $p_j(\mathbf{x})$ are monomials in the space coordinates $\mathbf{x}^T=[x,y]$, m is the number of polynomial basis functions, coefficients a_i and b_j are interpolation constants. In the RBF $R_i(r)$, the only variable is the distance between the interpolation point $\mathbf{x}$ and a field node $\mathbf{x}_i$, therefore, it is easy to be extended to 3-D problems. The second

term of Eq. (2) consists of polynomials to guarantee the non-singularity of the matrix and ensure linear completeness of the trial function (Liu and Gu, 2005).

There are a number of radial basis functions. In this paper, the following modified Multi-Quadrics (MMQ) RBF(Liu and Gu,2005) is used based on the local interpolation domain.

$$R_i(\mathbf{x}) = [r_i^2 + (\alpha_c d_c)^2]^q \tag{3}$$

where α_c is a dimensionless coefficient chosen, and d_c is a parameter of the nodal distance or nodal spacing. There are two parameters (α_c and q) to be predetermined. The effects of α_c and q have been thoroughly studied by Liu and Gu (2002). It has been found that α_c=4.0 and q=1.99 lead to good results for most problems considered. Hence, α_c=4.0 and q=1.99 will be used in this paper.

Coefficients a_i and b_i in Eq. (1) can be determined by enforcing Eq. (1) to be satisfied at the n nodes surrounding point $\mathbf{x}$. Hence, we can obtain:

$$\begin{bmatrix} \mathbf{u} \\ \mathbf{0} \end{bmatrix} = \begin{bmatrix} \mathbf{R_0} & \mathbf{P_m} \\ \mathbf{P_m^T} & \mathbf{0} \end{bmatrix}\begin{bmatrix} \mathbf{a} \\ \mathbf{b} \end{bmatrix} = \mathbf{Ga_0} \tag{4}$$

where,

$$\mathbf{P}_m^T = \begin{bmatrix} 1 & 1 & \cdots & 1 \\ x_1 & x_2 & \cdots & x_n \\ y_1 & y_2 & \cdots & y_n \end{bmatrix} \tag{5}$$

$$\mathbf{R}_0 = \begin{bmatrix} R_1(r_1) & R_2(r_1) & \cdots & R_n(r_1) \\ R_1(r_2) & R_2(r_2) & \cdots & R_n(r_2) \\ \vdots & \vdots & \ddots & \vdots \\ R_1(r_n) & R_2(r_n) & \cdots & R_n(r_n) \end{bmatrix} \tag{6}$$

Hence, we have

$$u^h(\mathbf{x}) = \mathbf{\Phi}^T(\mathbf{x})\mathbf{u}_e \tag{7}$$

where the shape function $\mathbf{\Phi}(\mathbf{x})$, as shown in Fig. 1, is defined by

$$\mathbf{\Phi}^T(\mathbf{x}) = \{R_1(r) \quad R_2(r) \quad \cdots \quad R_n(r) \quad 1 \quad x \quad y\}\mathbf{G}^{-1}$$

$$\mathbf{u}_e = \{u_1 \quad u_2 \quad \cdots \quad u_n \quad 0 \quad 0 \quad 0\}^T \tag{8}$$

Mathematicians have proven the existence of the RBF interpolation for arbitrarily scattered nodes (Schaback and Wendland, 2000). Therefore, the RBF interpolation usually has no interpolation singularity problem.
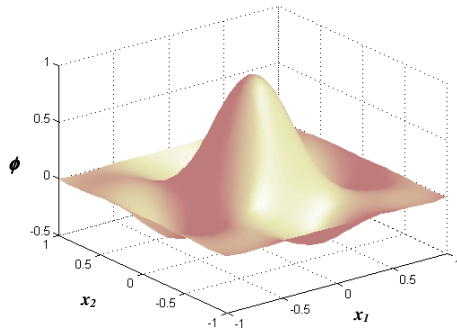
Figure 1: RBF shape function

However, the RBF meshless shape functions do not satisfy the continuity in the global domain (Liu and Gu, 2005). Because the smooth (or weight) function is not used in the RBF interpolation, some nodes will actually jump into or out of the interpolation domain. The approximated field function could be discontinuous when some nodes enter or leave the moving local interpolation domains. This discontinuity affects the computational accuracy of the meshless method based on RBFs. But fortunately, this negative influence is relative small for a local meshless method.

Discrete meshless formulations

Consider a body, as shown in Fig 2, which occupies a region $_0\Omega$ at the initial stage and occupies a region $_t\Omega$ at the step t. The deformation of a material particle $\mathbf{X} \in {}_0\Omega$ at time t is described by $\mathbf{x}(\mathbf{X},t) \in {}_t\Omega$ through the mapping functions $\boldsymbol{\varphi}$, and we have (Zienkiewicz and Taylor, 2000)

$$\mathbf{x} = \boldsymbol{\varphi}(\mathbf{X},t) = \mathbf{X} + \mathbf{u}(\mathbf{X},t) \tag{9}$$

where $\mathbf{u}$ is the displacement of this material particle. The deformation gradient $\mathbf{F}$ can be defined as

$$\mathbf{F} = \frac{\partial \boldsymbol{\varphi}}{\partial \mathbf{X}} = \frac{\partial \mathbf{x}}{\partial \mathbf{X}} = \frac{\partial \mathbf{u}}{\partial \mathbf{X}} + \boldsymbol{\delta} \tag{10}$$

Using the variables related to the current configuration, $_t\Omega$, the standard equilibrium equation for a solid is given by

$$\sigma_{ij,j} + \rho b_i = 0 \qquad \text{in } {}_t\Omega \tag{11}$$

where σ is the Cauchy stress tensor, b is the body force per unit mass and ρ is the mass density in the current configuration $_t\Omega$. In the current configuration, a symmetric measure of stress, the Cauchy (true) stress, σ, is often employed, which is the work conjugate of the rate-of-deformation, expressed as the relation with the second Piola-Kirchhoff stress, S

$$J\sigma_{ij} = F_{iI} S_{IJ} F_{jJ} \tag{12}$$

For the current configuration, the traction and displacement boundary conditions can be expressed as

$$\sigma_{ij} n_j = \bar{t}_i \quad on \; {}_t\Gamma_t \tag{13}$$

$$u_i = \bar{u}_i \quad on \; {}_t\Gamma_u \tag{14}$$

where $\mathbf{n}$ is the unit outward normal vector on the deformed surface, and $\bar{u}_i$ and $\bar{t}_i$ are prescribed displacements and tractions on the boundaries $_t\Gamma_u$ and $_t\Gamma_t$ of the current configuration $_t\Omega$.
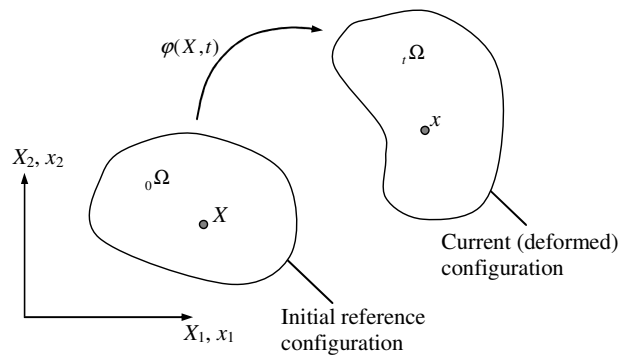

Figure 2: Reference and current configurations in the geometrically nonlinear analysis

Consider the equilibrium equation and the boundary conditions in the current configuration $_t\Omega$. For a field node L, Eq. (11) is satisfied by the Petrov-Galerkin formulation over a local quadrature domain $_t\Omega_q$ bounded by $_t\Gamma_q$ and leads to a local weak-form for this node, i.e.,

$$\int_{t\Omega_q} w_L(\sigma_{ij,j} + \rho b_i) \mathrm{d}_t\Omega = 0 \tag{15}$$

where w_L is the weight or test function centered usually at node L. The first part on the left-hand side of Eq. (15) can be integrated by parts to get

$$\int_{t\Gamma_q} w_L \sigma_{ij} n_j \mathrm{d}_t\Gamma - \int_{t\Omega_q} \left[w_{L,j} \sigma_{ij} - v_L \rho b_i \right] \mathrm{d}_t\Omega = 0 \tag{16}$$

Usually, the boundary $_t\Gamma_q$ for the local quadrature domain, $_t\Omega_q$, is composed by three parts, i.e., $_t\Gamma_q = {}_t\Gamma_{qi} \cup {}_t\Gamma_{qu} \cup {}_t\Gamma_{qt}$, where $_t\Gamma_{qi}$ is the internal boundary of the quadrature domain, which does not intersect with the global boundary $_t\Gamma$; $_t\Gamma_{qt}$ is the part of the natural boundary that intersects with the quadrature domain, and $_t\Gamma_{qu}$ is the part of the essential boundary that intersects with the quadrature domain. The spline weight function can be purposely selected so that the integral on $_t\Gamma_{qi}$ vanishes to simplify the local weak-form. Hence, the local weak-form of Eq. (16) can be re-written as

$$\int_{t\Omega_q} w_{L,j}\sigma_{ij}\mathrm{d}_t\Omega - \int_{t\Omega_q} w_L\rho b_i\mathrm{d}_t\Omega - \int_{t\Gamma_{qu}} w_L\sigma_{ij}n_j\mathrm{d}_t\Gamma$$
$$- \int_{t\Gamma_{qt}} w_L\overline{t_i}\mathrm{d}_t\Gamma = 0 \tag{17}$$

Due to the deformed configuration is unknown, the total Lagrangian (TL) formulation, which refers all stresses and deformations to the initial undeformed (reference) configuration at time $t=0$, is used. To get the formulations in the reference configuration, Eq. (17) can be re-written as the following matrix form

$$\int_{0\Omega_q} \mathbf{vFS}\mathrm{d}\Omega - \int_{0\Gamma_{qt}+0\Gamma_{qu}} \mathbf{wNFS}\mathrm{d}\Gamma = \int_{0\Gamma_{qt}} \mathbf{w}\overline{\mathbf{T}}\mathrm{d}\Gamma + \int_{0\Omega_q} \boldsymbol{\rho}\mathbf{wb}\mathrm{d}\Omega \tag{18}$$

To handle the large deformation, the incremental formulation is often used. For the reference (undeformed) configuration during a finite deformation, we have the following incremental relationships

$$^{t+dt}_{0}u_i = {}^t_0u_i + \Delta u_i ;$$
$$^{t+dt}_{0}S_{kj} = {}^t_0S_{kj} + \Delta S_{kj} ;$$
$$^{t+dt}_{0}F_{ik} = \frac{\partial^{t+dt}u_i}{\partial X_k} + \delta_{ik} = {}^t_0F_{ik} + \frac{\partial\Delta u_i}{\partial X_k} = {}^t_0F_{ik} + \Delta F_{ik} \tag{19}$$

Therefore, we can obtain the following incremental local weak-form in the matrix form

$$\int_{0\Omega_q} \mathbf{v}_L{}^t_0\mathbf{F}{}^t_0\mathbf{D}\Delta\mathbf{E}\mathrm{d}\Omega + \int_{0\Omega_q} \mathbf{v}_L{}^t_0\mathbf{S}\Delta\mathbf{F}\mathrm{d}\Omega$$
$$- \int_{0\Gamma_{qi}+0\Gamma_{qu}} \mathbf{w}_L{}^t_0\mathbf{N}{}^t_0\mathbf{F}{}^t_0\mathbf{D}\Delta\mathbf{E}\mathrm{d}\Gamma - \int_{0\Gamma_{qi}+0\Gamma_{qu}} \mathbf{w}_L{}^t_0\mathbf{N}{}^t_0\mathbf{S}\Delta\mathbf{F}\mathrm{d}\Gamma$$
$$= \int_{0\Gamma_{qt}} \mathbf{w}_L{}^t_0\overline{\mathbf{T}}\mathrm{d}\Gamma + \int_{0\Omega_q} \mathbf{w}_L\boldsymbol{\rho}\mathbf{b}\mathrm{d}\Omega + \int_{0\Gamma_{qi}+0\Gamma_{qu}} \mathbf{w}_L{}^t_0\mathbf{N}{}^t_0\mathbf{F}\widehat{\mathbf{S}}\mathrm{d}\Gamma$$
$$- \int_{0\Omega_q} \mathbf{v}_L{}^t_0\mathbf{F}{}^t_0\widehat{\mathbf{S}}\mathrm{d}\Omega \tag{20}$$

where $\mathbf{v}$ is the matrix for the derivatives of the weight functions, $\mathbf{F}$ is the deformation gradient matrix, $\Delta\mathbf{E}$ is the vector for the increments of Green strains, $\mathbf{S}$ and $\widehat{\mathbf{S}}$ are the matrix and the vector, respectively, of the second Piola-Kirchhoff stress, $\mathbf{N}$ is the matrix of the unit outward normal with respect to the reference configuration, and $\mathbf{D}$ is the material moduli with respect to the reference configuration.

Using the RBF meshless shape functions, the initial position vector $\mathbf{X}$, and the displacement vector $\mathbf{u}$ are approximated by the similar form. i.e.,

$$\mathbf{X} = \sum_{i=1}^n \Phi_i(\mathbf{X})\mathbf{X}_i \tag{21}$$

$$\mathbf{u} = \sum_{i=1}^n \Phi_i\mathbf{u}_i \tag{22}$$

Substituting Eqs. (21) and (22) into Eq. (20), we can obtain the discretized system of equations for the filed node L

$$\mathbf{K}_L\Delta\mathbf{U} = \mathbf{P}_L , \qquad L=1\sim N \tag{23}$$

where

$$\mathbf{K}_L = \int_{0\Omega_q} \mathbf{v}_L{}^t_0\mathbf{F}{}^t_0\mathbf{DB}^{nl}\mathrm{d}\Omega + \int_{0\Omega_q} \mathbf{v}_L{}^t_0\mathbf{SB}^l\mathrm{d}\Omega$$
$$- \int_{0\Gamma_{qi}+0\Gamma_{qu}} \mathbf{w}_L{}^t_0\mathbf{N}{}^t_0\mathbf{F}{}^t_0\mathbf{DB}^{nl}\mathrm{d}\Gamma - \int_{0\Gamma_{qi}+0\Gamma_{qu}} \mathbf{w}_L{}^t_0\mathbf{N}{}^t_0\mathbf{SB}^l\mathrm{d}\Gamma \tag{24}$$

$$\mathbf{P}_L = \int_{0\Gamma_{qt}} \mathbf{w}_L{}^t_0\overline{\mathbf{T}}\mathrm{d}\Gamma + \int_{0\Omega_q} \mathbf{w}_L\boldsymbol{\rho_0}\mathbf{b}\mathrm{d}\Omega$$
$$+ \int_{0\Gamma_{qi}+0\Gamma_{qu}} \mathbf{w}_L{}^t_0\mathbf{N}{}^t_0\mathbf{F}{}^t_0\widehat{\mathbf{S}}\mathrm{d}\Gamma - \int_{0\Omega_q} \mathbf{v}_L{}^t_0\mathbf{F}{}^t_0\widehat{\mathbf{S}}\mathrm{d}\Omega \tag{25}$$

where $\mathbf{D}$ is the material matrix, $\mathbf{F}$ is the deformation gradient matrix, $\mathbf{S}$ and $\widehat{\mathbf{S}}$ are, respectively, the matrix and the vector of the second Piola-Kirchhoff stress. Other matrices and vectors are given as

$$\mathbf{v}_L = \begin{bmatrix} w_{,x} & 0 & w_{,y} \\ 0 & w_{,y} & w_{,x} \end{bmatrix}, \qquad \mathbf{w}_L = \begin{bmatrix} w & 0 \\ 0 & w \end{bmatrix} \tag{26}$$

$$\mathbf{N} = \begin{bmatrix} N_x & 0 & N_y \\ 0 & N_y & N_x \end{bmatrix} \tag{27}$$

$$\overline{\mathbf{T}} = \begin{Bmatrix} \overline{T}_x \\ \overline{T}_y \end{Bmatrix}, \qquad \mathbf{b} = \begin{Bmatrix} b_x \\ b_y \end{Bmatrix} \tag{28}$$

$$\mathbf{B}^l = \begin{bmatrix} \dfrac{\partial\phi_1}{\partial X} & 0 & \cdots & \dfrac{\partial\phi_n}{\partial X} & 0 \\ 0 & \dfrac{\partial\phi_1}{\partial Y} & \cdots & 0 & \dfrac{\partial\phi_n}{\partial Y} \\ \dfrac{\partial\phi_1}{\partial Y} & 0 & \cdots & \dfrac{\partial\phi_n}{\partial Y} & 0 \\ 0 & \dfrac{\partial\phi_1}{\partial X} & \cdots & 0 & \dfrac{\partial\phi_n}{\partial X} \end{bmatrix} \tag{29}$$

$$\mathbf{B}^{nl} = \begin{bmatrix} F_{11}\dfrac{\partial\phi_1}{\partial X} & F_{21}\dfrac{\partial\phi_1}{\partial X} & \cdots \\ F_{12}\dfrac{\partial\phi_1}{\partial Y} & F_{22}\dfrac{\partial\phi_1}{\partial Y} & \cdots \\ F_{11}\dfrac{\partial\phi_1}{\partial Y}+F_{12}\dfrac{\partial\phi_1}{\partial X} & F_{21}\dfrac{\partial\phi_1}{\partial Y}+F_{22}\dfrac{\partial\phi_1}{\partial X} & \cdots \end{bmatrix} \tag{30}$$

It can be found that Eq. (23) is nonlinear because the right-hand side of this equation is also a function of displacements. Hence,

the Newton-Raphson iteration is used to get results in the analyses of large deformation problems. The iteration formulation can be written as (Belytschko et al., 2000)

$$\mathbf{U}^{(n+1)} = \mathbf{U}^{(n)} + \Delta\mathbf{U}^{(n)} \tag{31}$$

where $\mathbf{U}^{(n)}$ and $\mathbf{U}^{(n+1)}$ are displacements for the Newton-Raphson iteration at nth step and $(n+1)$th step, respectively, and $\Delta\mathbf{U}^{(n)}$ is the displacement increment, which can be computed as follows

$$\Delta\mathbf{U}^{(n)} = -\left(\mathbf{K}^{(n)}\right)^{-1}\mathbf{P}^{(n)} \tag{32}$$

NUMERICAL EXAMPLES

Uniaxial tension

A 1×0.25 plane strain block is subjected to tension along the axial direction, as shown in Figure 3. Symmetric boundary conditions are used to avoid rigid body motion. Regularly distributed 21, 36, and 55 nodes are used to study the convergence. To study the effectiveness and accuracy of the presented method, this problem is also solved using the finite element method with a very fine mesh (using 451 nodes). Because the theoretical solution for this problem is not available, the FEM result is taken as the reference solution. It is reasonable because the convergence of FEM has been proven both theoretically and practically. Hence, the following norm is defined as an error indicator,

$$e_u = \frac{\left|u_{(t)}^{Meshless} - u_{(t)}^{Ref}\right|}{\left|u_{(t)}^{Ref}\right|} \tag{33}$$

where $u_{(t)}^{Meshless}$ and $u_{(t)}^{Ref}$ are displacements obtained by the meshless method and the FEM reference solutions, respectively.

For easy comparisons, the axial displacement, u, at the end of the block is applied step by step. The displacement is increased by increments equal to Δu=0.2. After ten displacement steps, the block will stretch up to two times of its original length. The error, e_u, at the final deformed stage is smaller than 1%. It can be found that the present meshless method has very good accuracy, stability and convergence. It should be mentioned here that FEM solution converged much slower when the deformation becomes large.
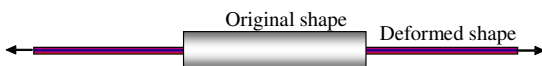

Figure 3: Deformation of a block under the uniaxial tension

Compression of a solid

A 4 ×2 solid billet, as shown in Fig. 4, is studied by the developed meshless method. This billet is subjected to compression along the axial direction. The large deformation analysis is performed and the billet is subjected to a distributed loading along the right end with 40/Unit. The analysis is carried out using load incremental steps N and the load-scaling factor is α=10.0. Fig. 5 plots the progression of deformations obtained by the meshless formulation for different loading steps. It is seen that the billet can be compressed as much as 75% compared to its original length. The same problem is also solved by the FEM and by the local Kriging method (Gu et al., 2007). It is found that the FEM will converge very slowly once the compression is more than 50%. It demonstrates that the meshless formulation developed in this paper is more effective than the FEM for the large deformation problems, and it has also proven that without using explicit mesh for both interpolation and integration, the local meshless method can fully overcome the mesh distortion issues in the FEM analysis.
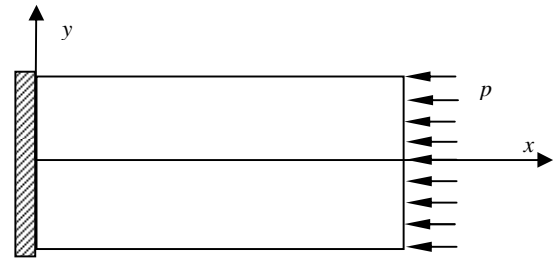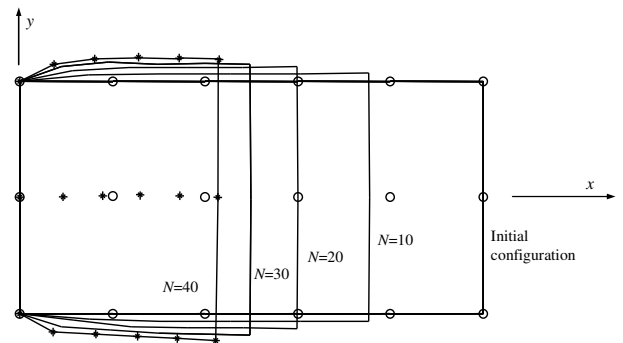

Figure 4: A solid bar under compression

O: Initial nodes; *: Deformed nodes after 40 steps

Figure 5: The compression progression for a billet

Ring compression

The compression of a metal ring, which is a typical problem in metal forming, is analyzed. As shown in Fig. 6, the initial ring

geometry is: internal radii: r_i =3.0 cm, height: h=4.0 cm, and external radii: r_e =6.0 cm. The ring is made of a cold forging steel with Young's modulus E=288 GPa and Poisson's ratio v=0.3.

Due to symmetry, only a quarter of the ring is discretized. Fig. 7 shows the ring progressive deformations under different compression rates. Comparing with results by ABAQUS and Chen et al. (1998), the present meshless technique leads to almost identified results.
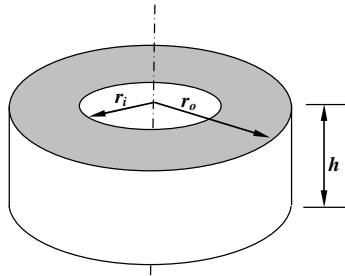


Figure 6: The metal ring

CONCLUSIONS

A local meshless formulation is developed for the large deformation analysis which is the key for the metal forming modelling. The radial basis function (RBF) is employed to construct the meshless shape functions. The discrete equations for large deformation of solids are obtained using the local weak-form, and based on the total Lagrangian (TL) approach, which refers all variables to the initial configuration. This formulation does not require explicit mesh in computation and therefore fully avoids mesh distortion difficulties in the large deformation analysis of metal forming. Several example problems are presented to demonstrate the effectiveness of the developed method in the large deformation analysis. It has been found that the present local meshless method has good performance, and it is also very stable even for irregularly distributed nodes. All these examples demonstrate that the present local meshless method is very effective for the large deformation analyses, because it fully avoids mesh distortion issues. In summary, the meshless techniques have very good potential in the modeling and simulation of metal forming problems.

ACKNOWLEDGEMENTS

REFERENCES

Atluri, SN and Shen, SP (2002). *The Meshless Local Petrov-Galerkin (MLPG) method*. Tech Sciemce Press. Encino USA.

Belytschko, T, Liu, WK and Moran, B (2000). *Nonlinear finite elements for continua and structures*. John Wiley & Sons, Chichester

Belytschko, T, Lu, YY and Gu, L (1994). "Element-Free Galerkin Methods," *International Journal for Numerical Methods in Engineering*, 37, pp 229-256.

Chen, JS, Pan, C, Wu, CT and Liu, WK (1996). "Reproducing kernal perticle methods for large deformation analysis of nonlinear structures," *Computer Methods in Applied Mechanics and Engineering*, 139, pp 195-227.

Chen, JS, Pan, C, Roque, CMOL and Wang, HP (1998). "A Lagrangian reproducing kernel particle method for metal forming analysis," *Computational Mechanics*, 22, pp 289-307.
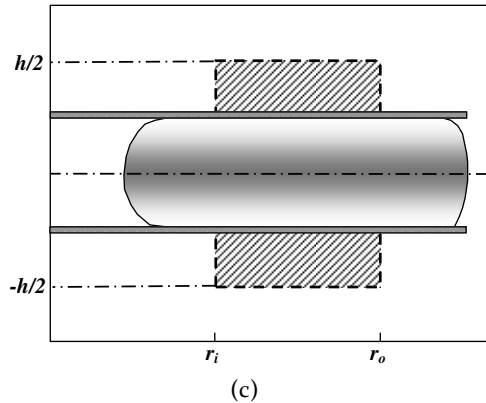
(a)

(b)

(c)
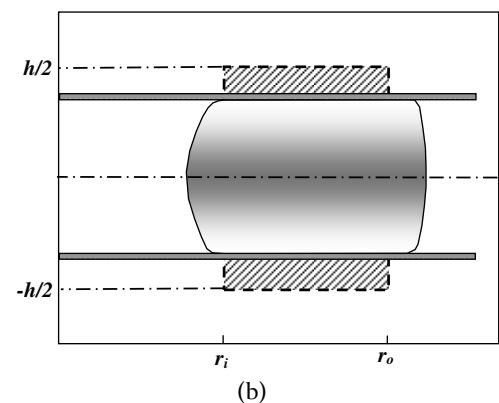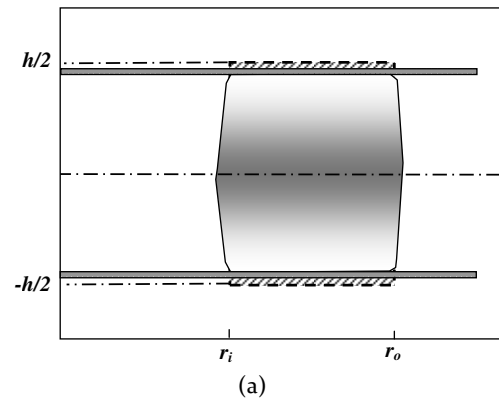
Figure 7: The compression progression for the ring

Gingold, RA and Moraghan, JJ (1977). "Smooth particle hydrodynamics: theory and applications to non spherical stars," *Monthly Notices of the Royal Astronomical Society*, 181, pp 375-389.

Gu, YT and Liu, GR (2001a). "A meshless Local Petrov-Galerkin (MLPG) formulation for static and free vibration analyses of thin plates," *CMES-Computer Modeling in Engineering & Sciences*, 2(4), pp 463-476.

Gu, YT and Liu, GR (2001b). "A meshless local Petrov-Galerkin (MLPG) method for free and forced vibration analyses for solids," *Computational Mechanics*, 27 (3), pp 188-198.

Gu, YT and Liu, GR (2001c). "A local point interpolation method for static and dynamic analysis of thin beams," *Computer Methods in Applied Mechanics and Engineering*, 190, pp 5515-5528.

Gu, YT, Wang QX, and Lam KY(2007). "A Meshless Local Kriging Method for large deformation Analyses," *Computer Methods in Applied Mechanics and Engineering*, 196, pp 1673–1684.

Jun, SA(1996). "Meshless method for nonlinear solid mechanics," *RIKEN Review*, 14, 33-34.

Liu, GR and Gu, YT (2001a). "A point interpolation method for two-dimensional solids," *International Journal for Numerical Methods in Engineering*, 50, pp 937-951.

Liu, GR and Gu, YT (2001b), A local radial point interpolation method (LR-PIM) for free vibration analyses of 2-D solids. *Journal of Sound and Vibration*, 246(1), pp 29-46.

Liu, GR and Gu, YT (2002). "Comparisons of two meshfree local point interpolation methods for structural analyses," *Computational Mechanics*, 29(2), pp 107-121.

Liu, GR and Gu, YT (2005). *An introduction to meshfree methods and their programming*. Springer Press, Berlin.

Liu, WK, Jun, S, and Zhang, Y (1995). "Reproducing kernel particle methods" *International Journal for Numerical Methods in Engineering*, 20, pp 1081-1106.

Schaback, R and Wendland, H (2000). "Characterzation and construction of radial basis functions," *Multivariate Approximation and Applications*(eds.) N. Dyn, D. Leviatan, D. Levin & A. Pinkus, Cambridge University Press.

Zienkiewicz OC and Taylor RL (2000). *The finite element method* (5th ed.). Butterworth Heinemann, Oxford.